Title	Observation of fast sound in metal-nonmetal transition in liquid Hg
Auther(s)	Inui, Masanori; Ishikawa, D.; Tamura, K.; Tsutsui, S.; Baron, A.P.R.
Citation	Journal of Physics and Chemistry of Solids , 66 (12) : 2223 - 2229
Issue Date	2005-12
DOI	10.1016/j.jpcs.2005.09.021
Self DOI	
URL	http://ir.lib.hiroshima-u.ac.jp/00040638
Right	(c)2005 Elsevier Ltd. All rights reserved.
Relation	

Observation of fast sound in metal-nonmetal transition in liquid Hg

M. Inui[1], D. Ishikawa[2], K. Matsuda[3], K. Tamura[3], S. Tsutsui[4] and A.Q.R. Baron[4]

[1]Faculty of Integrated Arts and Sciences, Hiroshima University, Higashi-Hiroshima 739-8521, Japan

[2]SPring-8/RIKEN 1-1-1 Kouto, Mikazuki-cho, Sayo-gun, Hyogo-ken, 679-5148, Japan

[3]Graduate School of Engineering, Kyoto University, Kyoto, 606-8501, Japan

[4]SPring-8/JASRI 1-1-1 Kouto, Mikazuki-cho, Sayo-gun, Hyogo-ken, 679-5198, Japan

Abstract

Liquid Hg undergoes the metal-nonmetal (M-NM) transition when it is expanded from 13.6 g cm^{-3} at ambient conditions to 9 g cm^{-3} at high temperature and high pressure. To investigate collective and single particle motions in expanded fluid Hg, we have made inelastic x-ray scattering experiments and obtained the dynamic structure factor, $S(Q,\omega)$, of fluid Hg. We analyzed $S(Q,\omega)$ within the framework of generalized hydrodynamics and found that the excitation energies of collective modes disperse three times as fast as the hydrodynamic sound velocity in the M-NM transition region at 9 gcm^{-3}. The results indicate the existence of fast sound in expanded fluid Hg accompanying the metal-non-metal transition and strongly hint that fluctuations intrinsic to the M-NM transition are induced on atomic length scale and sub-picosecond time scale.

Corresponding Author:

Masanori INUI

Faculty of Integrated Arts and Sciences, Hiroshima University

Higashi-Hiroshima, 739-8521, Japan

Tel. (81) (0)824-24-6555

Fax. (81) (0)824-24-0757

e-mail: inui@mls.ias.hiroshima-u.ac.jp

1. Introduction

The metal-nonmetal (M-NM) transition has been one of significant subjects in physics. A simple band picture predicts that a divalent metal should be transformed to an insulating state with volume expansion. Among divalent metals, liquid Hg is the most proper element to study the M-NM transition with volume expansion along the saturated vapor pressure curve because its critical constants are within temperatures and pressures experimentally accessible (critical data of Hg [1]: T_C = 1751 K, P_C = 1673 bar, ρ_C = 5.8 g cm^{-3}). The first indication of the M-NM transition was found in the electrical conductivity and thermopower data obtained by Hensel and Frank [2] and fluid Hg undergoes the M-NM transition with decreasing density, ρ, from 13.6 g cm^{-3} at ambient conditions to 9 g cm^{-3} near the critical point. Figure 1 shows the phase diagram of fluid Hg on the temperature and pressure plane. A bold solid curve denotes the saturated vapor-pressure curve and the open circle at the end is the liquid-vapor critical point. The isochors are denoted by thin solid lines. The bold broken line denotes the isochors where the M-NM transition occurs. After several band calculations failed to explain a band crossing M-NM transition at 9 g cm^{-3} [3-6], Kresse and Hafner [7] succeeded in opening the gap between 6s and 6p bands at the exact densities with local structure consistent with that experimentally obtained by Tamura and Hosokawa [8]. Studies on expanded fluid metals including fluid Hg were reviewed by Hensel and Warren [9].

The study of the dynamical properties is of great importance to understand the mechanism of the M-NM transition in fluid Hg. In the last decade, the use of inelastic x-ray scattering (IXS) at third generation synchrotron radiation sources has allowed many new studies of the dynamics of disordered materials. A remarkable result among them may be strikingly similar collective dynamics between van der Waals and metallic fluids, suggesting the universality of the short time dynamics in monatomic liquids [10]. Compared to these liquids, expanded fluid Hg is non-simple. In fact, inhomogeneous regime [11] or two-state model [12] were proposed to explain the electronical and thermodynamic properties of fluid Hg in the M-NM transition region. Fluctuations near the critical point may also play an essential role for the M-NM transition. We measured IXS spectra of expanded fluid Hg from the liquid to dense vapor and observed an anomaly of collective dynamics in the M-NM transition region. We reported the results of dense vapor [13] and the fluid

in the M-NM transition [14] in letters. In this paper, we report these results briefly and discuss the details of collective dynamics in the M-NM transition at 9 g cm^{-3} based on results newly obtained from the framework of generalized hydrodynamics using memory function formalism.

2. Experimental

This work has been done at the high-resolution IXS beamline (BL35XU) of SPring-8 in Japan [15]. Backscattering at the Si (11 11 11) reflection was used to provide a beam of 3×10^9 photons/sec in a 0.8 meV bandwidth onto the sample. The energy of the incident beam and the Bragg angle of the backscattering were 21.747 keV and 89.98°, respectively. We used three spherical analyzer crystals at the end of the 10 m horizontal arm to analyze the scattered x-rays. The spectrometer resolution was 1.6-1.8 meV (slightly degraded because our large high-pressure vessel forced the detectors about 240 mm away from the sample position) and the momentum transfer resolution was ΔQ = 1nm^{-1}. The Hg sample of 99.999 % purity and 0.024 mm thickness for the M-NM transition and 0.1 mm thickness for the dense vapor was mounted in a single-crystal sapphire cell [16] and He gas of 99.9999 % purity was used as a pressurizing medium.

Figure 2 (a) shows a side view of the internally-heated high-pressure vessel installed at BL35XU. The vessel can be operated up to 2000 K and 2000 bar after being fixed in a frame made of a super-high tension steel which is not shown in the figure. Thanks to a large sample space, we could mount the vessel on the sample table of the high-resolution spectrometer at BL35XU. As shown in Fig.2 (b), the vessel had three Be windows of 10 mm diameter and 10 mm thickness for scattered x rays and five smaller windows of 4mm diameter and 5mm thickness for incident ones. So the x-rays traveled through 15 mm of Be, 150 mm of He (at high pressure) and the 0.024 (0.1) mm sample. We can measure different scattering angles by choosing different angle set-up. At the present experiments, the windows were centered at scattering angles of 2θ = 1°, 5 °, 10 °, 15 °, 19 ° and 24 °, or from 2 to 48.3 nm^{-1} and the 10 mm diameter windows permitted the simultaneous use of 3 analyzer crystals. For the crucial low momentum transfer, Q, near the M-NM transition at 9 g cm^{-3}, we collected several data sets at different vessel rotations relative to the very small (0.1mm in diameter) incident beam. This allowed access to a small range of momentum transfers near to 2

nm^{-1}. We measured IXS spectra for expanded fluid Hg at thermodynamic states (T [K], p [bar], ρ [g cm^{-3}]) of (298, 2, 13.6), (773, 50, 12.4), (1273, 500, 11.0), (1723, 1940, 9.0), (1723, 1398, 3.0), (1623, 1023, 2.1) and (1423, 510, 1.0) and those at 2θ of 1^o at several densities from 9 to 4 g cm^{-3}. He gas contributed significant background, especially at low Q. The backgrounds were measured at each pressure and temperature, and were subtracted after being scaled for sample transmission. The transmission data were also used to estimate the density of the fluid sample. The signal from fluid Hg became so large at low Q with volume expansion that we have succeeded in obtaining good quality data. At present, we believe that the subtraction of the background succeeded in giving reasonable spectra of fluid Hg because as shown in Fig.3 in Ref. [14], we could observe clear difference in dynamical sound velocity of fluid Hg at densities between 9 and 8 g cm^{-3} near the M-NM transition region where there was only small temperature difference by 30-40 degrees at the same high pressure.

3. Results

Figure 3 shows selected IXS data at 13.6, 9 and 2 g cm^{-3}. Thermodynamic states of these densities are shown by open squares in Fig.1. After the subtraction of background with absorption correction, the integral, $S(Q)$, of the spectrum, $S(Q,\omega)$, was used for the normalization, and $S(Q,\omega)/S(Q)$ are plotted in the figure. The resolution function obtained from a measurement of a poly methyl methacrylate (PMMA) is shown by a solid curve at the bottom. The spectra at ambient condition at 13.6 g cm^{-3} have a clear side peak at around 10 meV at Q around 10 nm^{-1}. The spectra agree well with those reported by Hosokawa et al [17]. The IXS spectra at 9.0 g cm^{-3} have a single peak and the side peaks not distinct from the central one. The peak at 2 nm^{-1} at 9 g cm^{-3} is as sharp as that at 2 g cm^{-3}. The central peaks at 37.1 and 46.8 nm^{-1} are much broader at the M-NM transition at 9.0 g cm^{-3} than at ambient conditions, 13.6 g cm^{-3} and they are very similar to those at 2 g cm^{-3} at the same Q.

4. Analysis

We analyzed the data in the framework of generalized hydrodynamics [18]. Here to investigate the microscopic dynamics in detail, we analyzed the data using generalized Langevin formalism [19,20].

The intermediate scattering function, *F(Q,t)*, which is the time-Fourier transform of *S(Q,ω)*, obeys the following equation.

$$\ddot{F}(Q,t)+\frac{\omega_0^2(Q)}{S(Q)}F(Q,t)+\int_0^t M(Q,t-t')\dot{F}(Q,t')dt'=0. \qquad (4.1)$$

Here the quantity $\omega_0^2(Q)/S(Q)=k_BTQ^2/mS(Q)$ is related to the generalized isothermal sound velocity through the relation $c_t(Q)=\sqrt{\omega_0^2(Q)/Q^2S(Q)}$. The classical dynamic structure factor, *S(Q,ω)*, can be expressed in terms of a complex memory function *M(Q, t)*. According to the results utilized in a simple liquid by a molecular dynamics simulation [19] and several liquid metals [20,21], we adopted a simple exponential decay for a fast relaxation process (μ-process) and the structural relaxation process (α-process) given by,

$$\begin{aligned} M(Q,t)=&\left(\omega_\ell^2(Q)-\frac{\gamma\omega_0^2(Q)}{S(Q)}\right)\left[(1-A_\alpha(Q))\exp(-t/\tau_\mu(Q))+A_\alpha(Q)\exp(-t/\tau_\alpha(Q))\right] \\ &+(\gamma-1)\frac{\omega_0^2(Q)}{S(Q)}\exp(-D_T(Q)Q^2t) \end{aligned} \qquad (4.2)$$

Here the parameters, $\tau_\mu(Q)$, $\tau_\alpha(Q)$ and $A_\alpha(Q)$ are the fast and structural relaxation times, and the fraction of the α-process , respectively. The thermal diffusivity $D_T(Q)=K/\rho C_V$ is given by the thermal conductivity, *K*, density, *ρ*, and the specific heat at a constant volume, C_V. The parameters, $\omega_\ell(Q)$ and γ are the normalized fourth moment of *S(Q,ω)* and the specific heat ratio, respectively. The generalized infinite-frequency sound velocity is given by $c_\infty(Q)=\omega_\ell(Q)/Q$. Using the Fourier-Laplace transform of *M(Q, t)*, $\tilde{M}(Q,-i\omega)$, an expression of *S(Q,ω)* is obtained as follows,

$$\left[S(Q,\omega)/S(Q)\right]^{model}=\frac{1}{\pi}\mathrm{Re}\left[\frac{\omega_0^2(Q)/\left(\omega^2S(Q)\right)}{-i\omega+\dfrac{\omega_0^2(Q)}{-i\omega S(Q)}+\tilde{M}(Q,-i\omega)}\right] \qquad (4.3).$$

To fit the model function with the experimental data, the above function modified by the detailed balance condition was convoluted with the resolution function *R(ω)*.

$$S(Q,\omega)/S(Q) = \int \frac{\hbar\omega'/k_BT}{1-\exp(-\hbar\omega'/k_BT)} E(Q)\left[S(Q,\omega')/S(Q)\right]^{\mathrm{mod}\,el} R(\omega-\omega')d\omega' \qquad (4.4)$$

We introduced another parameter *E(Q)* adjustable to the amplitude of S(Q,ω) /S(Q) and it was converged to be 1 ± 0.1. We took $\gamma = 3$ and the value of C_V from macroscopic data [22] for the fluid at 9 g cm^{-3}. We estimated the *K* of fluid Hg at 9 g cm^{-3} using Wiedemann-Franz law, $K/\sigma T = const.$, and the conductivity (σ) data [1]. The estimated *K* at 9 g cm^{-3} was about 1/4 as large as *K* at the ambient condition. Then we fixed the thermal diffusivity at 9 g cm^{-3} as the value of $D_T(Q) = 1.8\times10^{-6}$ m^2 s^{-1} obtained from these macroscopic quantities and estimated the time constant of thermal decay, $\tau_h^{-1}(Q) = D_T(Q)Q^2$. We have numerical data of *S(Q)* at 9 g cm^{-3} [23] but they are not so reliable at low *Q*. Thus we left it to an optimized parameter. Consequently, we carried out the least-square fitting of the experimental data and optimized the parameters, *E(Q)*, *S(Q)*, $\omega_\ell(Q)$, $\tau_\mu(Q)$, $\tau_\alpha(Q)$ and $A_\alpha(Q)$. In the least-square fitting, the $\tau_\mu(Q)$ was optimized near the initial value of 1 fs. This means that the μ-process becomes a frequency-independent friction parameter in the present analysis and we should have used the memory function simplified by using just an adjustable constant with a delta function like the equation shown in Ref. [10]. Thus we do not comment the μ-process in the next section. Figure 4 shows the fits of the experimental data at 3.4 nm^{-1} and 9 g cm^{-3}. We calculated the longitudinal current-current correlation function, $J(Q,\omega) = (\omega^2/Q^2)S(Q,\omega)^{\mathrm{mod}\,el}$, using the deconvoluted $S(Q,\omega)^{model}$ and defined the excitation energy of the sound mode, $\omega_p(Q)$, as the peak position of $J(Q,\omega)$. The effective sound speed, $c_s(Q)$ were deduced from the equations, $c_s(Q) = \omega_p(Q)/Q$. In this paper, energy [meV] divided by 0.658 gives angular frequency [ps^{-1}].

5. Discussion

The $\omega_p(Q)$ (closed circles) at 9 g cm^{-3} are plotted as a function of *Q* in Fig.5 together with the excitation energy of the sound mode, Ω_Q (open squares), previously reported using a DHO model [14]. Both results are reasonably consistent with each other. The excitation energy has a minimum near Q_M = 23 nm^{-1}of the *S(Q)* maximum, which is well-known as de-Gennes narrowing. Figure 6 shows $c_s(Q)$ (closed circles) at 9 g cm^{-3} as

a function of Q. Also shown are the $c_t(Q)$ (open triangles) and $c_\infty(Q)$ (open squares). The values of $c_s(Q)$ at low Q are distributed around 1500 m s^{-1}, which is three times larger than the ultrasonic sound speed of about 490 m s^{-1} [24,25]. Speeding up the effective sound velocity in liquids with increasing Q has been understood as the transition from hydrodynamic to viscoelastic regime. In the hydrodynamic limit, $\omega\tau << 1$ (ω;angular frequency, τ;relaxation time), the effective sound velocity approaches to $c_t(Q)$ while it has the limit of $c_\infty(Q)$ in the case $\omega\tau >> 1$.

We discuss the characteristic time scale of the relaxation in the sound mode at 9 g cm^{-3}. Figure 7 shows the optimized parameters of $A_\alpha(Q)$ and $\tau_\alpha(Q)$ as a function of Q, and the estimated $\tau_h(Q)$ as a reference. In the measured Q region, the $A_\alpha(Q)$ takes the value from 0.7 to 0.95. This means that structural relaxation (slow relaxation) is dominant compared with the μ process. As expected from the fast sound at low Q, $\tau_\alpha(Q)$ at low Q has a large value of 0.2 to 0.3 ps on average. In fact, the quantity, $\omega_p(Q)\tau_\alpha(Q)$ becomes about 1 at low Q as shown in the inset of Fig.7, which means that the structural process derives an effective increase of the sound speed at low Q. The $\tau_\alpha(Q)$ seems to decrease rapidly with increasing Q. At higher Q, $\tau_\alpha(Q)$ becomes about one order smaller than at low Q and remains almost constant. The effective sound speed $c_s(Q)$ close to $c_t(Q)$ may be explained by the fact of $\omega_p(Q)\tau_\alpha(Q) < 1$ at high Q. At 9 g cm^{-1}, $\gamma = 3$ may be too large to ignore the effect of thermal relaxation process. The estimated $\tau_h(Q)$ at low Q has almost as large as $\tau_\alpha(Q)$ at the same Q but the thermal effect is expected to be fully relaxed at higher Q. These results may indicate that the structural effect dominantly contributes the fast sound at low Q and the thermal effect may contribute partially.

In the present analysis using the memory function formalism, however, we were aware of a curious behavior of a fitting parameter. Figure 8 shows $S(Q)$ at 9 g cm^{-1} as a function of Q. Open and closed circles denote the optimized $S(Q)$ and the $S(Q)$ obtained from the integration of observed $S(Q,\omega)$, respectively. $S(Q)$ obtained from x-ray diffraction [23] is shown by a solid curve. At Q higher than 10 nm^{-1}, the open and closed circles agree reasonably with the solid line. However, the optimized $S(Q)$ (open circles) at low Q seems systematically smaller than the static ones experimentally obtained as seen in the inset of Fig.8. The $S(Q)$

from x-ray diffraction may not be reliable because Q is too low to be measured by wide angle x-ray scattering but recent data of small angle x-ray scattering for expanded fluid Hg [26] also supported $S(Q)$ of about 0.4 at 3 nm^{-1}. These results hint that unrealistic small $S(Q)$ is needed to reproduce the fast sound at low Q within the memory function formalism though we have to note that the formalism conserves zeroth, second and fourth frequency moments of $S(Q,\omega)$.

There is another inconsistency with the macroscopic data. The $c_t(Q)$ related to $S(Q)$ in Fig.6 shows the effective adiabatic sound velocity derived from $c_t(Q)$ times $\sqrt{\gamma}$ is much larger than the ultrasonic sound velocity at low Q. For comparison, we analyzed the data of fast sound in water at the ambient condition [27] using the same formalism. The velocities obtained from optimized parameters were $c_t(Q)$ = 1400 m s^{-1}, $c_s(Q)$ = 2900 m s^{-1}, and $c_\infty(Q)$ = 3500 m s^{-1} at 4 nm^{-1}. The $c_t(Q)$ times $\sqrt{\gamma}$ ($\gamma \approx 1$ for ordinary water) seems consistent with the ultrasonic sound velocity of 1500 m s^{-1}, which does not show inconsistency like the case of expanded fluid Hg in the M-NM transition. The optimized $S(Q)$ of 0.07 at 4 nm^{-1} agrees fairly well with the one of 0.06 reported for water [28]. These results may mean that the fast sound observed at low Q in expanded fluid Hg couldn't exactly be described using the memory function formalism for a classical liquid.

Next we investigated how parameters change when $S(Q)$ was fixed to be the value experimentally obtained. As an example, the fits at 3.4 nm^{-1} (taking $S(Q)$ = 0.4) are shown in Fig.9 (a) (the same data in Fig.4). Despite similar optimization, the χ^2 remains large and the tail of the peak is not well reproduced in Fig. 9 (a). The optimized $\omega_p(Q)$ was 1.3 meV, corresponding to $c_s(Q)$ of about 600 m s^{-1}. This velocity is close to the ultrasonic sound velocity of 490 m s^{-1}. Similar results were obtained for $S(Q,\omega)$ at low Q besides Q = 2 nm^{-1}. as shown in the inset of Fig.6. Both of $c_t(Q)$ and $c_\infty(Q)$ in the inset take reasonable values. Larger values of $S(Q)$ pulled down the isothermal sound velocity $c_t(Q)$ to about 400 m s^{-1} and it may result in smaller $c_s(Q)$ close to the ultrasonic sound velocity. To see the additional mode at higher energy, we tried to carry out the fits using a model function constituted from the sum of the memory function and a DHO term. The result is shown in Fig.9 (b). The excitation energy of the DHO term was 3.2 meV, corresponding to $c_s(Q)$ of about

1400 m s^{-1}. The DHO term appears to reproduce the fast sound. The peaks from the memory function seem to become sharp. After averaging results at several Q, $A_\alpha(Q)$ and $\tau_\alpha(Q)$ were obtained about 0.4 and about 1 ps, respectively. We do not stress these values because the last model function may be artificial. The results of the present analysis using the memory function formalism may be summarized as follows. When we fix the input parameters deduced from the experimental ($Q \to 0$, or $\omega \to 0$) values, the present memory function formalism presented the results consistent with the hydrodynamic sound whose velocity is a little larger than the ultrasonic sound velocity. It is similar to 'positive dispersion' observed in many liquids. The mode with higher excitation energy observed as fast sound must arise from another mechanism. Alternatively, by a release of the constraint of $S(Q)$ the memory function formalism could represent the fast sound but some parameters seemed to become physically unacceptable. We need further analysis and consideration to conclude these results.

Is there any possibility that the fast sound observed at low Q appears in fluid Hg accompanying the M-NM transition? First we point out a possibility of an additional mode having an origin similar to a formation of dimeric molecules in the M-NM transition in expanded fluid Rubidium reported by Pilgrim et al. [29]. However divalent Hg has the electronic configuration of a closed shell like helium and hardly forms dimetic molecules in gaseous state though a Hg_2 molecule is known to exist. The additional modes must have an origin from another type of aggregate in fluid Hg. Then let us consider a microscopic dynamics in fluid Hg accompanying the M-NM transition. The results of x-ray diffraction experiments suggest that the average number of nearest neighbors within the first coordination shell around an atom is reduced with volume expansion, while the nearest neighbor distance remains unchanged [8, 23]. When the coordination number decreases, a change of a single particle motion is expected. In ambient conditions at 13.6 g cm^{-3}, the line shape of $S(Q,\omega)$ at high Q is similar to a Lorentzian function, which suggests that diffusive motion is dominant in the liquid. With decreasing density, the line shape at high Q broadens and it becomes very similar to those at 2 g cm^{-3}, as seen in Fig.1. This suggests that at 9.0 g cm^{-3} a free particle motion is dominant over short (less than interatomic) distances like the dense vapor. In the generalized hydrodynamics

for classical liquids, the fast sound as the limit to $c_\infty(Q)$ does not obey the standard relation, $\chi_s = 1/(\rho v_s^2)$, where χ_s is the adiabatic compressibility, and v_s velocity of normal sound because $c_\infty(Q)$ is related to infinite-frequency limits of both bulk and shear moduli like a solid. However in consideration of the mechanism of the present fast sound observed at the M-NM transition as an additional mode, let us use the simple equation $\chi_s = 1/(\rho v_s^2)$. The fast sound velocity suggests that the microscopic χ_s is much smaller than the macroscopic one, which means that the mean square fluctuations of microscopic pressure, $\left\langle (\Delta p)^2 \right\rangle = k_B T V^{-1} \chi_s^{-1}$, are very large. The enhancement of microscopic $\left\langle (\Delta p)^2 \right\rangle$ can be caused by a local deformation of a pair potential, $\phi(R, n_e)$, especially its repulsive part, as shown by the pressure equation for a liquid metal [30],

$$p = n_i k_B T + n_i n_e \frac{du_0}{dn_e} - \frac{N n_i}{2} \int \left\{ \frac{R}{3V} \frac{\partial \phi(R, n_e)}{\partial R} - \frac{n_e}{V} \frac{\partial \phi(R, n_e)}{\partial n_e} \right\} g(R) d\mathbf{R} \qquad (5.1)$$

where n_i and n_e denote number densities of ions and conduction electrons, respectively, *g(R)* a pair distribution function, and u_0 the energy of conduction electrons. We expect such a deformation in a pair potential being enhanced at the M-NM transition, due to the large fluctuations of local electronic states between metallic and insulating ones. A sign of fluctuations at the M-NM transition may be found in the present data in Fig. 3 such as the narrowing of *S(Q,ω)* for 2.0 nm^{-1} at 9.0 g cm^{-3} compared with at ambient conditions, and rapid increase of *S(Q)* at low *Q* with $Q \to 0$ in Fig. 8. In addition, when the pressure exerted from conduction electron denoted by a density derivative of u_0 in eq. (5.1) is taken into account, the enhancement of $\left\langle (\Delta p)^2 \right\rangle$ may be promoted more. Aggregates of atoms largely coordinated may have metallic nature and those of less coordinated atoms insulating. Such inhomogeneous regime may be induced in the M-NM transition. We speculate that the inhomogeneous regime in the M-NM transition exists within a microscopic length scale and sub-picosecond time scale and that it is different from long range fluctuations in a particle number, $\left\langle (\Delta N)^2 \right\rangle$, near the liquid-vapor critical point. Thus the appearance of the fast sound strongly hints that the M-NM transition accompanies intrinsic fluctuations induced by the local deformation of a pair potential and the pressure provided by conduction electrons.

6. Summary

We carried out inelastic x-ray scattering measurements for expanded fluid Hg and found fast sound in the M-NM transition. Within the framework of generalized hydrodynamics, we could obtain useful information on the fast sound at 9 g cm^{-3} from the present analysis using the memory function formalism. When the fast sound observed at low Q could be reproduced well within the memory function formalism, the parameter of $S(Q)$ became unrealistic smaller than the one experimentally obtained. It resulted in giving unacceptable isothermal sound velocity $c_t(Q)$. On the other hand, when the experimental $S(Q)$ was taken in the fitting procedure, the memory function formalism represented microscopic sound waves in '*molecular hydrodynamic*' region which may be extended from the ultrasonic sound waves but did not reproduce the additional mode with higher excitation energy, the fast sound. We consider that the latter interpretation may be more plausible and speculate that the fast sound is originated from fluctuations in the pair potential or the pressure derived from electron gas, which are intrinsic to the M-NM transition. Although the mechanism of the observed fast sound is not fully understood at present, we can stress that the fluid in the M-NM transition in liquid Hg must be a fruitful example of non-simple liquids that have an anomalous dynamics.

Acknowledgements

The authors would like to thank Prof. K. Hoshino, Prof. F. Shimojo, Prof. S. Hosokawa and Dr. T. Scopigno for their va1uable discussion. The authors are grateful to Dr. T. Ishikawa and Dr. Y. Tanaka for their support of this project. Kobe Steel Co. Ltd. and High Pressure System Co. Ltd. are acknowledged for their technical support. This work is supported by the Grant-in-Aid for Specially Promoted Research from the Ministry of Education, Science and Culture of Japan under contract No. 11102004. The synchrotron radiation experiments were performed at the SPring-8 with the approval of the Japan Synchrotron Radiation Research Institute (JASRI) (Proposal No.2003A6607-LD-np and 2003B0206-ND3d-np).

References

[1] W. Goezlaff, G. Schoenherr, and F. Hense1, Z. Phys.. Chem. NF **156**, 219 (1988), W. Goezlaff, *PhD Thesis, University of Marburg* (1988).

[2] F. Hensel and E. U. Franck, Ber. Bunsenges. Phys. Chem. **70**, 1154 (1966).

[3] M. A. C. Devillers and R. G. Ross, J. Phys. F **5**, 73 (1975).

[4] H. Overhof, H. Uchtmann and F. Hensel, J. Phys. F **6**, 523 (1976).

[5] P. Fritzson and K. -F. Berggren, Solid State Commun., **19**, 385 (1976).

[6] L. F. Mattheis and W. W. Warren, Jr., Phys. Rev. B **16**, 624 (1977).

[7] G. Kresse and J. Hafner, Phys. Rev. B **55**, 7539 (1997).

[8] K. Tamura and S. Hosokawa, Phys. Rev. B **58**, 9030 (1998).

[9] F. Hensel and W. W. Warren, Jr., *Fluid Metals* (Princeton University Press, New Jersey, 1999)

[10] T. Scopigno, A. Filipponi, M. Krisch, G.. Monaco, G.. Ruocco and F. Sette, Phys. Rev. Lett. **89**, 255506 (2002).

[11] M. H. Cohen and J. Jortner, Phys. Rev. A **10**, 978 (1974).

[12] M. Ross and F. Hensel, J. Phys.: Condens. Matter **8**, 1909 (1996).

[13] D. Ishikawa, M. Inui, K. Matsuda, K. Tamura, A.Q.R. Baron, S. Tsutsui, Y. Tanaka and T. Ishikawa, J. Phys.: Condens. Matter, **16**, L45 (2004).

[14] D. Ishikawa, M. Inui, K. Matsuda, K. Tamura, S. Tsutsui and A.Q.R. Baron, Phys. Rev. Lett. **93**, 097801 (2004).

[15] A. Baron, Y. Tanaka, D. Miwa, D. Ishikawa, T. Mochizuki, K. Takeshita, S. Goto, T. Matsushita, H. Kimura, F. Yamamoto and T. Ishikawa, Nucl. Inst. Methods A **467-468**, 627 (2001).

[16] K. Tamura, M. Inui and S. Hosokawa, Rev. Sci. Instrum. **70**, 144 (1999).

[17] S. Hosokawa, H. Sinn, F. Hensel, A. Alatas, E.E. Alp, W.-C. Pilgrim, J. Non-Cryst. Solids **312-314**, 163 (2002).

[18] J. P. Boon and S. Yip, *Molecular Hydrodynamics* (McGraw-Hill, New York, 1980).

[19] D. Levesque, L. Verlet and J. Kurkjiarvi, Phys. Rev. A **7**, 1690 (1973).

[20] T. Scopigno, U. Balucani, G.. Ruocco and F. Sette, J.Phys.: Condens. Matter **12**, 8009 (2000).

[21] T. Scopigno, U. Balucani, G.. Ruocco and F. Sette, Phys. Rev. E **63**, 011210 (2000).

[22] M. Levin and R. Schmutzler, J. Non-Cryst. Solids, **61& 62**, 83 (1984).

[23] M. Inui, X. Hong, and K Tamura, Phys. Rev. B **68**, 094108 (2003).

[24] M. Yao, K. Okada, T. Aoki, and H. Endo, J. Non-Cryst. Solids, **205-207**, 274 (1996).

[25] V. Kozhevnikov, D. Arnold, E. Grodzinskii, S. Naurzakov, J. Non-Cryst. Solids, **205-207,** 256 (1996).

[26] M.Inui, K.Matsuda, D.Ishikawa, K. Tamura and Y. Ohishi, private communication.

[27] T. Yamaguchi, K. Yoshida, N. Yamamoto, S. Hosokawa, M. Inui, S. Tsutsui and A.Q.R. Baron, "Collective dynamics of supercritical water", in this proceedings.

[28] L. Bosio, J. Teixeira and H.E. Stanley, Phys. Rev. Lett. **46**, 597 (1981).

[29] W.-C. Pilgrim, M. Ross, L.H. Yang and F. Hensel, Phys. Rev. Lett. **78**, 3685 (1997).

[30] M. Hasegawa and M. Watabe, J. Phys. Soc. Jpn, **32**, 14 (1972).

Figure Captions

Fig.1

Phase diagram of fluid Hg. The bold solid curve denotes the saturated vapor pressure curve and the open circle is the critical point. The isochore at 9 g cm^{-1} is indicated by a bold broken line. Open squares denote thermodynamic states whose spectra are shown in Fig.3.

Fig.2

(a) a side-view of a high-pressure vessel for inelastic x-ray scattering experiments.

(b) a top-view of the high-pressure vessel.

Fig.3

Dynamic structure factor, $S(Q,\omega)/S(Q)$, of fluid Hg at 13.6, 9 and 2 g cm^{-3}. A peak denoted by a solid curve at the bottom is a resolution function. The $S(Q,\omega)/S(Q)$ at 2 g cm^{-3} is multiplied by 0.5 at Q from 2.4 to 19.8 nm^{-1} for exhibition.

Fig.4

An example of the least-square fits at 3.4 nm^{-1} at 9 g cm^{-3}. Open circles denote experimental data and the optimized convoluted model function is shown by a bold solid curve. Also shown are the resolution function (thin broken curve) and the model function (thin solid curve).

Fig.5

Dispersion relation of fluid Hg at 9 g cm^{-3}. The ω_p and Ω_Q [14] are indicated by closed circles and open squares, respectively.

Fig.6

Sound velocities, $c_s(Q)$ (closed circles), $c_t(Q)$ (open triangles) and $c_\infty(Q)$ (open squares) at 9 g cm^{-3} as a function of Q. The inset indicates the velocities optimized by taking experimental $S(Q)$ at low Q (see text).

Fig.7

The optimized $A_\alpha(Q)$ and $\tau_\alpha(Q)$and $\tau_h(Q)$ estimated from the macroscopic data at 9 g cm^{-3} as a function of Q. The inset indicates $\omega_p(Q)$ times $\tau_\alpha(Q)$ as a function of Q up to 22 nm^{-1}.

Fig.8

$S(Q)$ at 9 g cm^{-3}. Open circles denote the optimized ones obtained from the fitting. Closed circles are the properly normalized integrals of $S(Q,\omega)$ experimentally observed. Also shown is $S(Q)$ (a solid curve) obtained from x-ray diffraction experiments [23]. The inset shows low Q region on an enlarged scale.

Fig.9

Example of the least-square fitting with fixed $S(Q)$ at 3.4 nm^{-1} at 9 g cm^{-3} using the memory function (a) and the sum of the memory function and a DHO term (b).

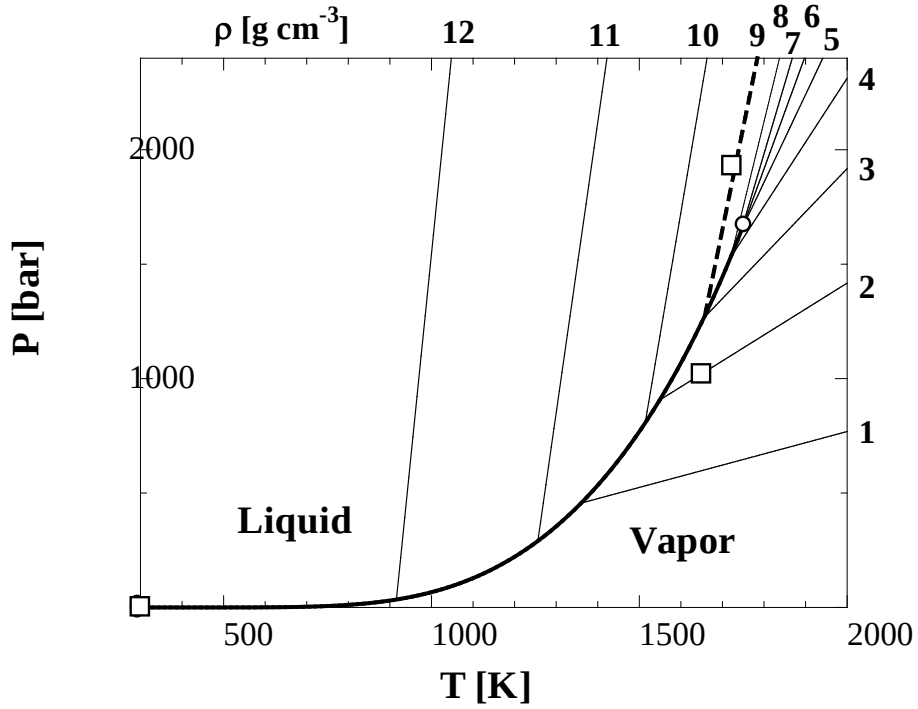
ρ [g cm-3]
12
11
10
9
8
7
6
5
4
3
2
1
2000
1000
P [bar]
Liquid
Vapor
500
1000
1500
2000
T [K]

Fig.1

(a)

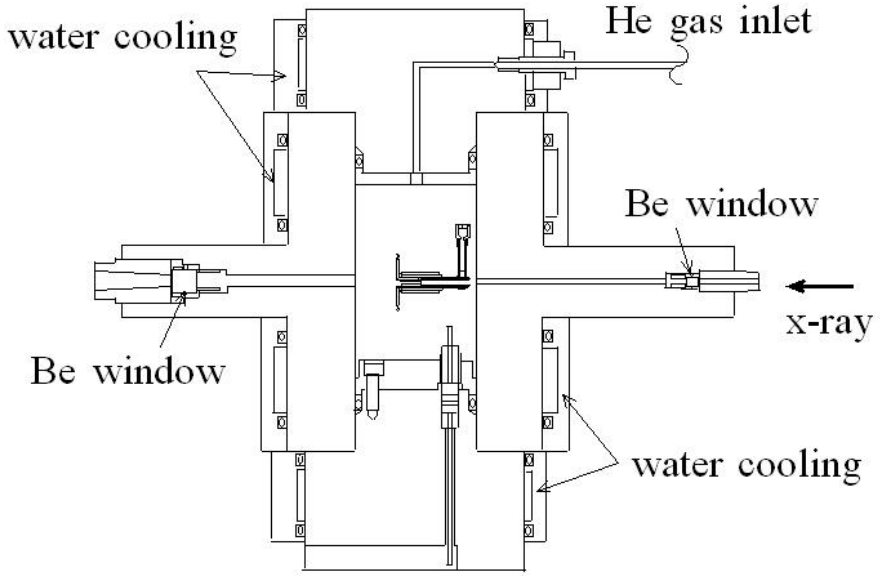
water cooling
He gas inlet
Be window
x-ray
Be window
water cooling

(b)

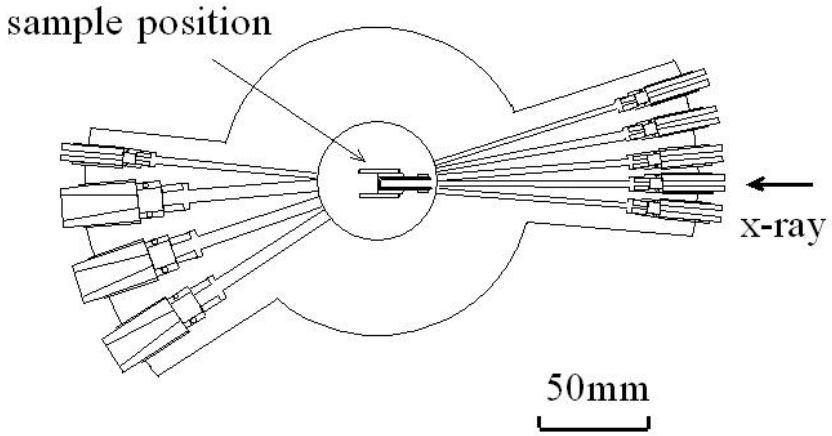
sample position
x-ray
50mm

Fig.2

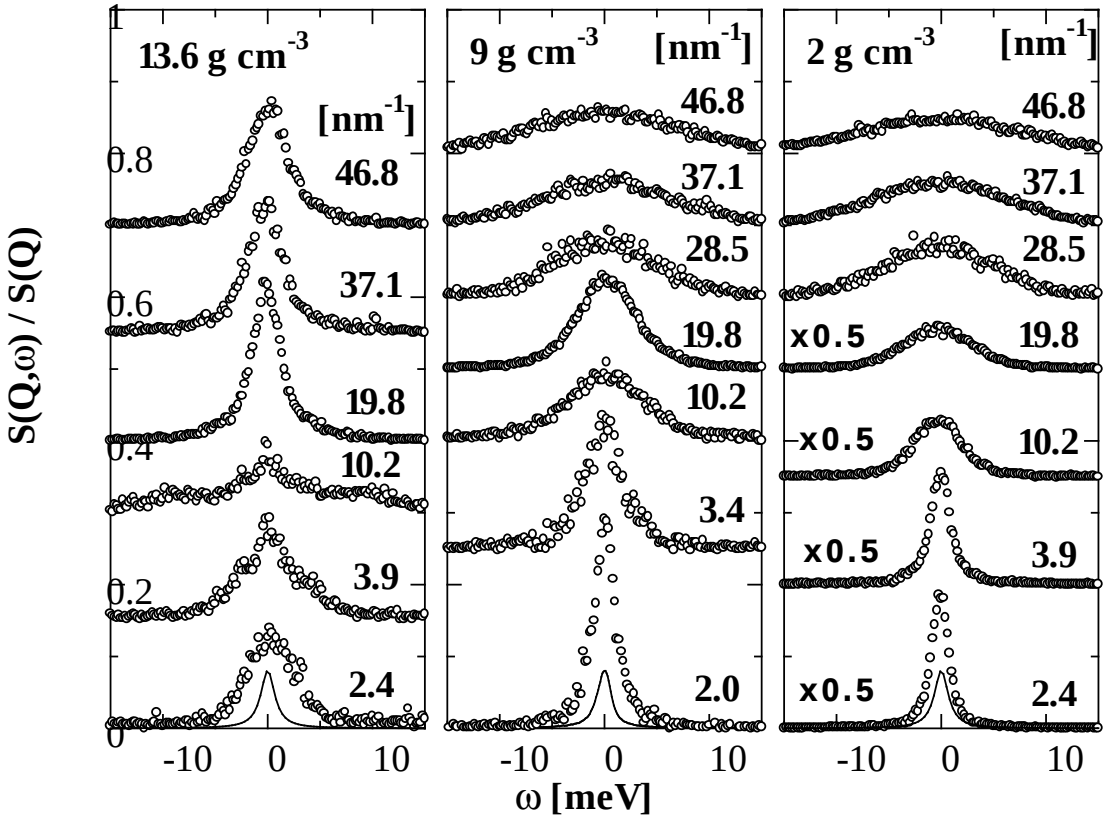
13.6 g cm-3
9 g cm-3
2 g cm-3
[nm-1]
46.8
37.1
28.5
19.8
10.2
3.9
2.4
3.4
2.0
x0.5
S(Q,ω) / S(Q)
ω [meV]
-10
0
10
0.2
0.4
0.6
0.8
1

Fig.3

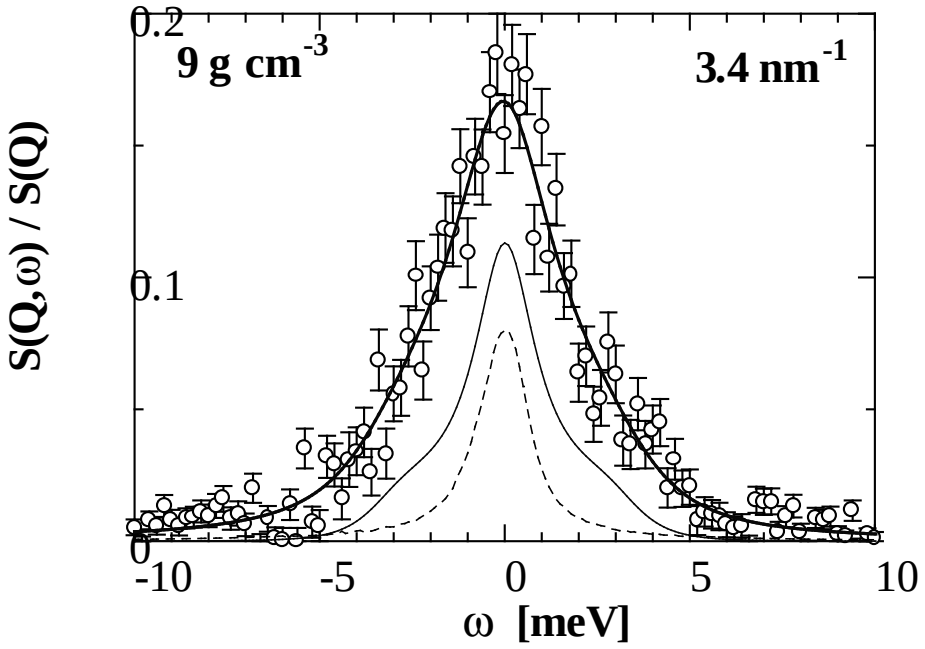

Fig.4

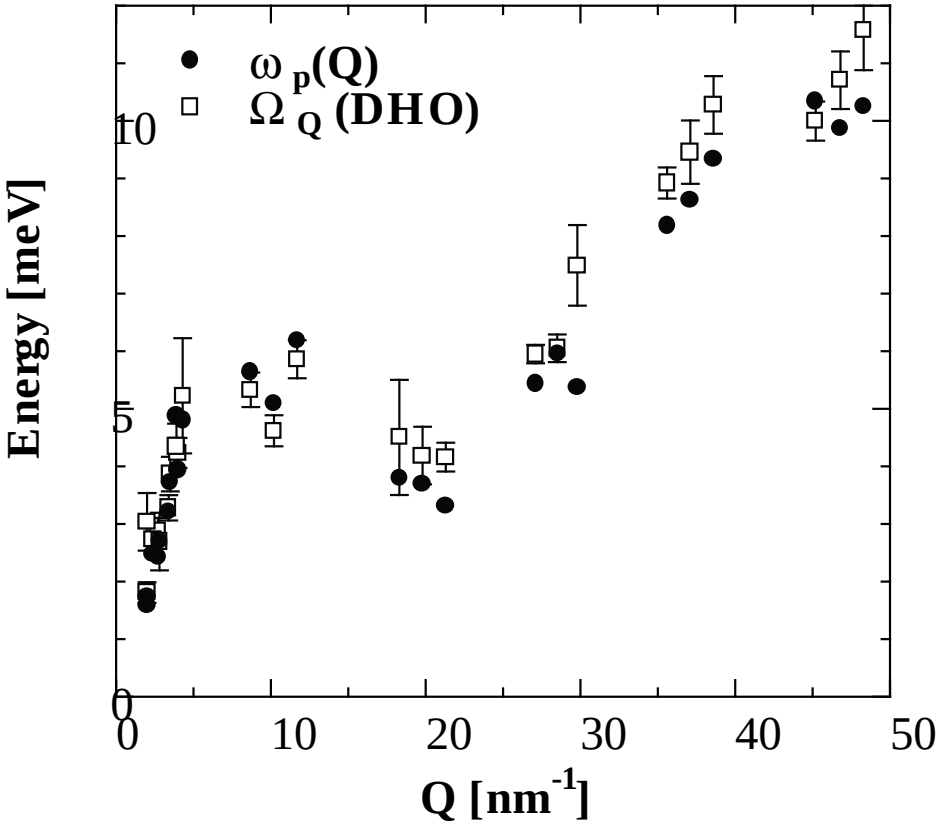

Fig.5

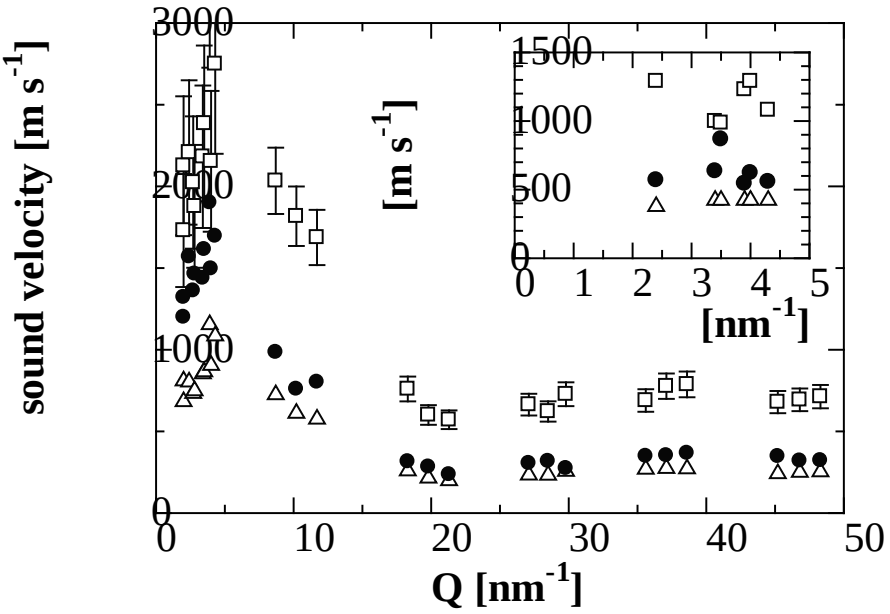
sound velocity [m s-1]
3000
2000
1000
0
0
10
20
30
40
50
Q [nm-1]
[m s-1]
1500
1000
500
0
0
1
2
3
4
5
[nm-1]

Fig.6

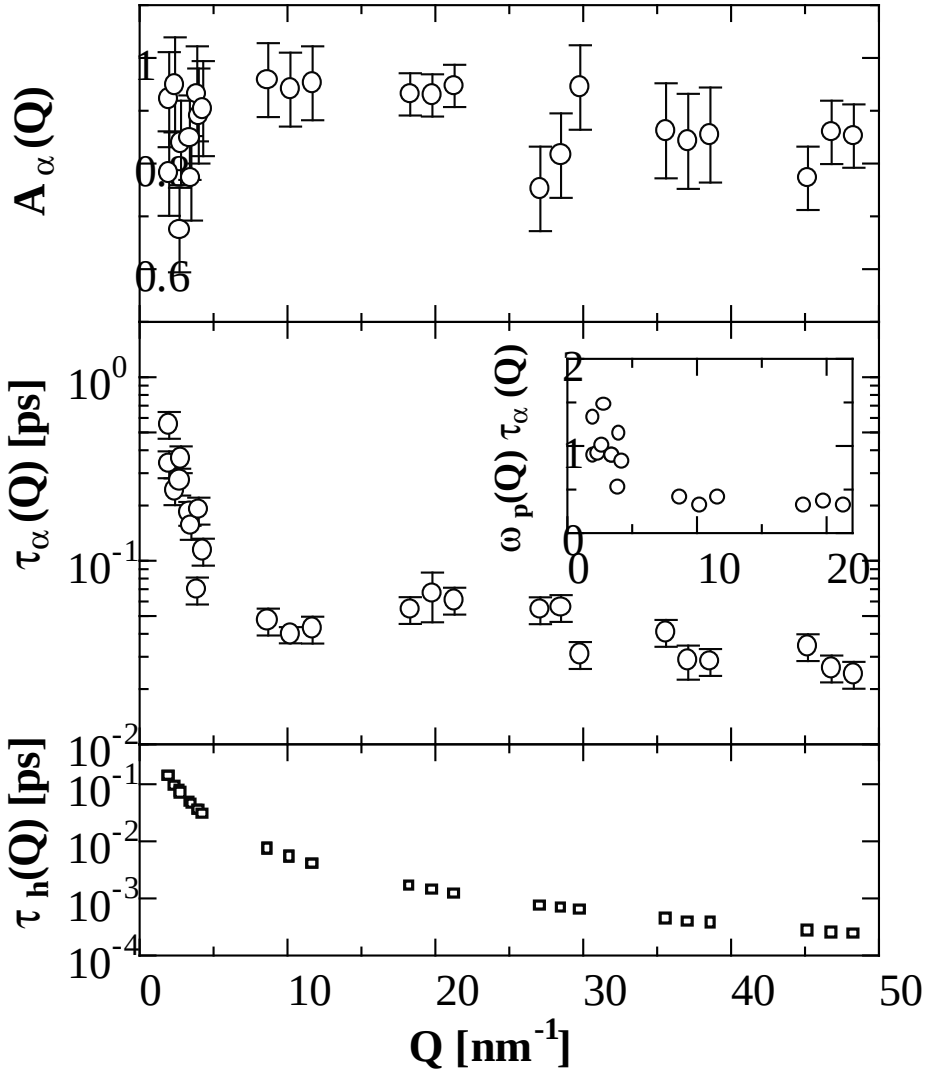
A α (Q)
1
0.6
τ α (Q) [ps]
10^0
10^-1
10^-2
ω p(Q) τ α (Q)
2
1
0
0
10
20
τ h(Q) [ps]
10^-1
10^-2
10^-3
10^-4
0
10
20
30
40
50
Q [nm^-1]

Fig.7

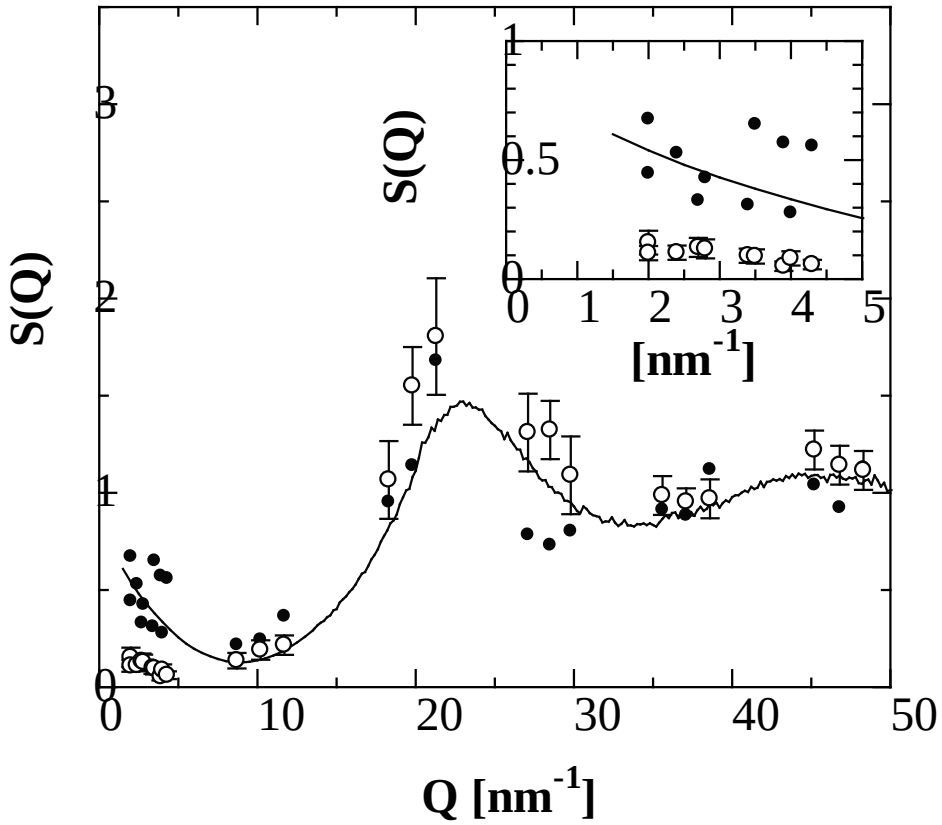

Fig.8

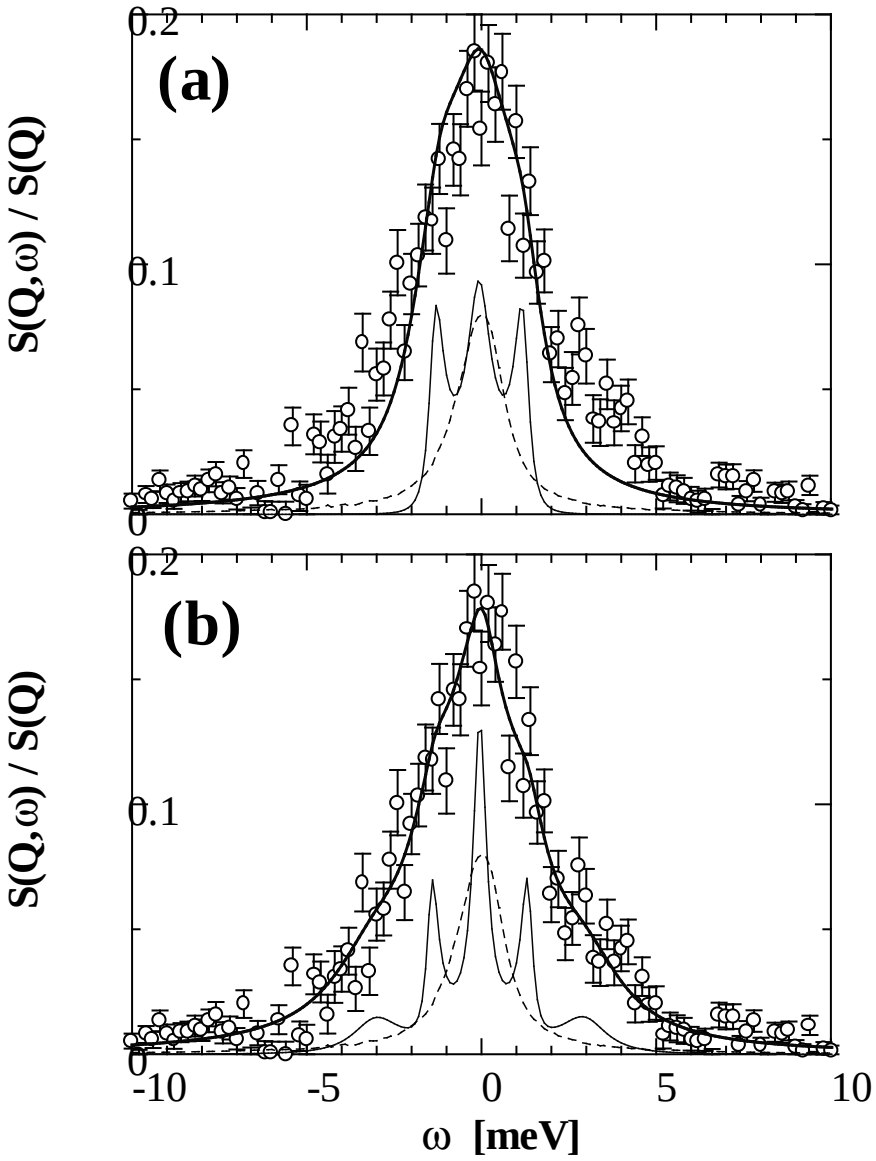

Fig.9

Length estimation

Title, abstract, author affiliation (two col.)	11.5 cm	483 words
Body		4016 words
9 Figures (one col.)	76.6 cm (estimated total height)	1610 words
	total	6109 words